

Supporting Information

An All-Optical Excitonic Switch Operated in the Liquid and Solid Phases

*Donald L. Kellis,[‡] Christopher Sarter,[‡] Brittany L. Cannon, Paul H. Davis, Elton Graugnard,
Jeunghoon Lee, Ryan D. Pensack, Theresa Kolmar, Andres Jäschke,^{*} Bernard Yurke,^{*} and
William B. Knowlton^{*}*

[‡]These authors contributed equally.

^{*}Email: bknowlton@boisestate.edu, bernardyrurke@boisestate.edu, jaeschke@uni-hd.de.

Table of Contents:

S1. Switching contrast, cyclic fatigue, cycle time, modulation, and photostability	4
S2. Phosphoramidite synthesis	5
Scheme S1. Photoswitchable phosphoramidite reaction pathway	5
Table S1. DNA sequences	6
S3. Normalized spectral overlap and chromophore selection	7
Figure S1. Spectral overlap	8-9
S4. Single photochromic nucleotide switching efficiency	10
Figure S2. HPLC switching efficiency chromatogram	10
Table S2. HPLC switching efficiency gradient	11
S5. Absorbance of one <i>versus</i> three photochromic nucleotide	12
Figure S3. Saw-tooth plots	13-14
S6. Fluorescence measurements	15
Figure S4. Detector geometry	16
S7. Controls	17-18
Figure S5. Controls plots	19
S8. Solid phase concentration calculations	20-22

Figure S6. Solid phase profilometry	23-24
Table S3. Liquid and Solid phase concentration	24
S9. Solid phase variation	24
S10. Switching time derivation	25-27
S11. Characteristic switch time derivation	28-33
S12. Time trial design	34
Table S4. Summed exposure times	35
S13. Absorbance cross section	36
S14. Photon energy, photon fluence, and photon flux	37-38
S15. Ultrafast laser switching	39
S16. All-optic switch to 14 nm node FinFET comparison	40-41
Table S5. Bulk 14 nm FinFET parameters	42
Table S6. All-optical excitonic switch parameters	43-44
S17. Photochromic nucleotide synthesis, attachment, and purification	45-47
Table S7. Nucleotide modification	48
Table S8. Mass, sequence, and chemical formula	48
Table S9. HPLC purification gradients	49

Table S10. LC/MS gradient	49
Figure S7. HPLC chromatograms	49
References	50

Supplementary Text:**S1: Switching contrast, cyclic fatigue, cycle time, modulation, and photostability**

We define the following terms for the discussion of the all-optical excitonic switch. ON/OFF switching contrast denotes the difference between the ON state static emission and the OFF state static emission of either the donor or the acceptor. Cyclic fatigue indicates any undesirable changes in the donor or the acceptor emission as a result of repeated ON/OFF cycling. Cycle time describes the time of exposure to a given wavelength of light (*i.e.*, 300 nm or 455 nm) used to cycle the all-optical excitonic switch between the closed or open configurations, respectively. Modulation refers to a statistically significant variation in donor or acceptor emission between the ON and OFF states. Photostability refers to the limited irreversible degradation of chromophores.

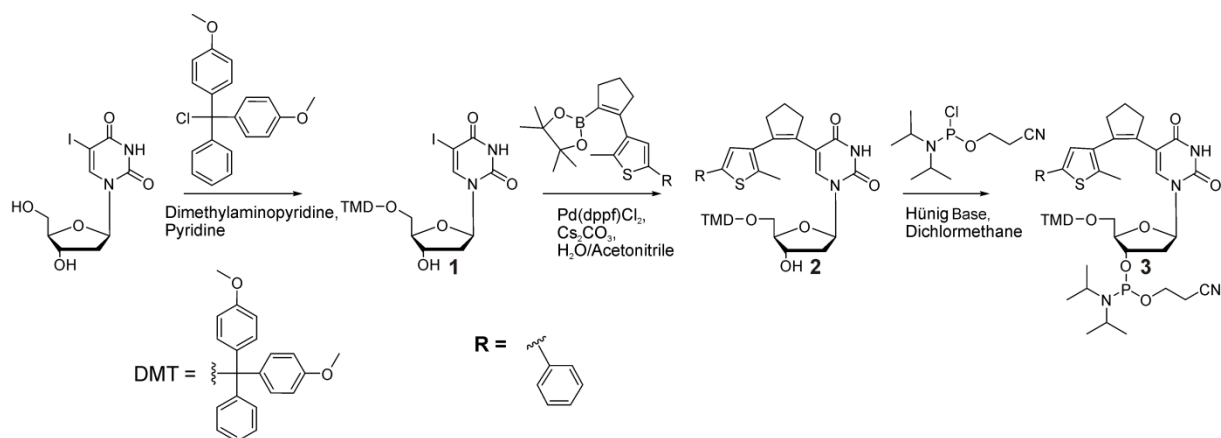
S2: Synthesis of the phosphoramidite for solid phase synthesis**Scheme S1:** Reaction pathway to synthesize the photoswitchable phosphoramidite building block**(3)** needed for solid phase synthesis.

Table S1: Single strand DNA sequences

Strand Name	Sequence (5' to 3')	Length (nt)	Purification
Photochromic Strand (1) – PS1	GGCTAGCTACdU ^{PS} ACGA	15	HPLC ^a
Photochromic Strand (3) – PS3	GGCTAGCdU ^{PS} ACdU ^{PS} ACdU ^{PS} A	15	HPLC ^a
Donor Strand	/A390/AGTAGTAGCTAGCCGCACGCACCGGCTCG	29	Dual HPLC ^a
Acceptor Strand	CGAGCCGGTGCGTGC/A488/	15	Dual HPLC ^a
Photochromic (control)	GGCTAGCTACTACTA	15	Standard Desalting ^b
Donor (control)	AGTAGTAGCTAGCCGCACGCACCGGCTCG	29	Standard Desalting ^b
Acceptor (control)	CGAGCCGGTGCGTGC	15	Standard Desalting ^b

a: High-Performance Liquid Chromatography

b: Desalting to remove short products and small organic contaminants. Does not include polyacrylamide gel electrophoresis (PAGE) purification.

The common name and structure of the chromophores used in this study are:

ATTO 390: (2,5-dioxopyrrolidin-1-yl) 4-(4,6,8,8-tetramethyl-2-oxo-6,7-dihydropyrano[3,2-g]quinolin-9-yl)butanoate.

ALEXA 488: Xanthylum, 3,6-diamino-9-[2-carboxy-4(*or* 5)-[(2,5-dioco-1-pyrrolidinyl)oxy]carbonyl]phenyl]-4,5-disulfo-, inner salt, lithium salt (1:2) (39).

S3: Normalized and unaltered spectral overlap data and chromophore selection

As indicated by the corresponding arrows in Figure S1a, which presents normalized absorption and emission spectra of all chromophores present in the all-optical excitonic switch, the chromophores were selected such that facile excitonic transfer occurs between the ATTO 390 donor emission ($\lambda_{\text{max}} = 460$ nm, solid blue curve) and Alexa 488 acceptor absorption ($\lambda_{\text{max}} = 495$ nm, dashed green curve). Additionally, the donor emission and the acceptor absorption fall well within the broad absorption band of the photochromic nucleotide when it is in the closed (“OFF” state) configuration (Fig. S1a, red dashed curve, 388 – 550 nm). For additional clarity in understanding the relative absorbance of the acceptor and photochromic nucleotide moieties, which affects the overall switching efficiency (*i.e.*, FRET modulation) of the all-optical excitonic switch, Figure S1b presents the unaltered (*i.e.*, non-normalized) absorption spectra of the Alexa 488 acceptor strand as well as the three photochromic nucleotide switch in its open and closed configurations, with the peak emission wavelength of the ATTO 390 donor indicated. Note that the absorbance of the photochromic nucleotides is ~6x less than that of the acceptor at the donor’s emission maximum, which leads to incomplete FRET quenching in the all-optical excitonic switch’s OFF state (*i.e.*, partial modulation of the fluorescence emission).

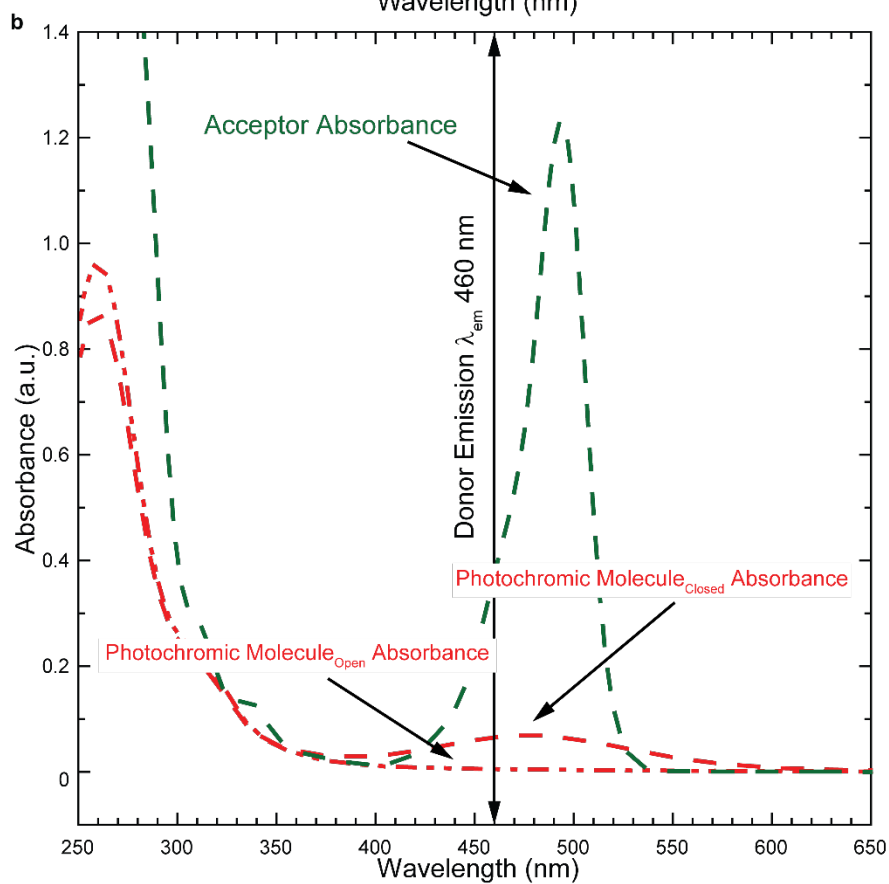
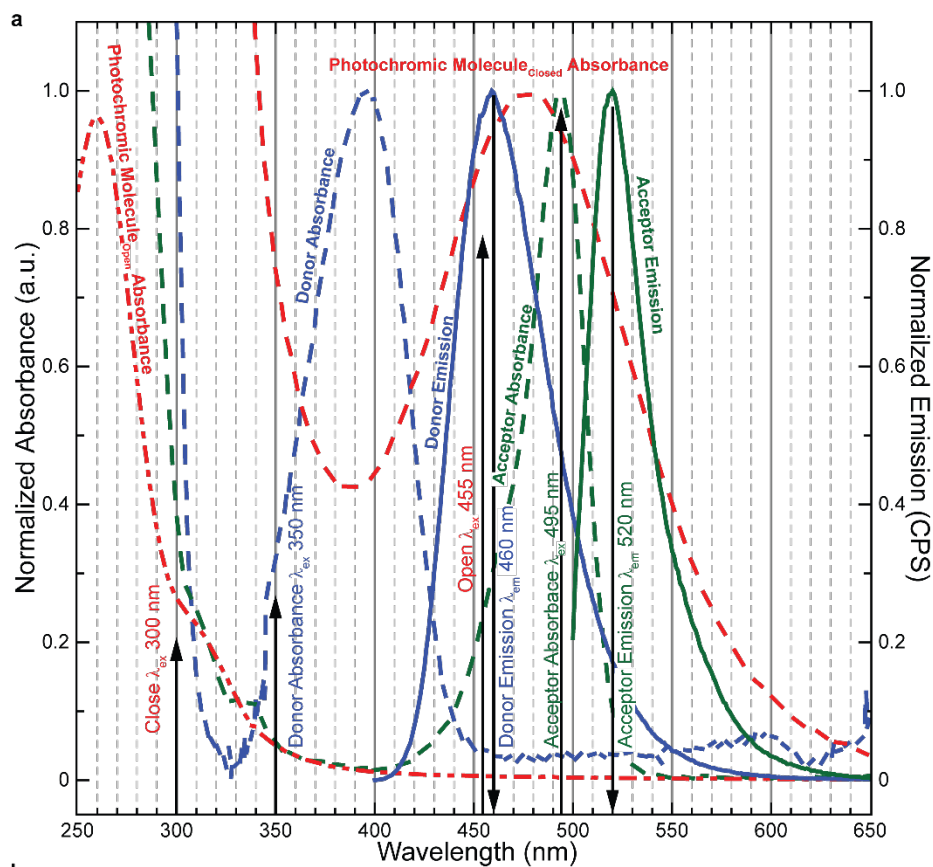


Figure S1. Spectral overlap of the optical components comprising the all-optical excitonic switch.

(a) Shown are the normalized absorption and emission spectra of the donor strand (blue dashed and solid curves, respectively), normalized absorption spectra of the photochromic nucleotides in both the open (non-absorbing, red dashed/dotted curve) and closed (absorbing, red dashed curve) configurations, and normalized absorption and emission spectra of the acceptor strand (green dashed and solid curves, respectively). Optical molecules were selected such that overlap occurred among the donor emission, photochromic nucleotide closed configuration absorption, and acceptor absorption in order to modulate both the excitonic transfer and FRET processes. Exposure wavelengths were chosen such that minimal perturbation to the configuration of the photochromic nucleotides would occur during data collection. Up arrows indicate the wavelengths used to expose the optical molecule and the down arrow indicates the wavelength used to collect spectral data. The spectra have been normalized in order to easily visualize the spectral overlap in the 350-550 nm region. (b) The actual unaltered absorbance of the acceptor as well as the three photochromic nucleotides in their open and closed states. A comparison of the spectra highlights that the absorbance of the three photochromic nucleotides at the donor emission maximum ($\lambda_{max} = 460$ nm) is approximately 6x lower than the acceptor. The vertical double-headed arrow indicates the donor's peak emission wavelength of 460 nm.

S4: Determination of the switching efficiency of **PS1** (quantitative composition of the photostationary state)

The switching efficiency was determined by irradiating **PS1** for 10 min with a 310 nm LED in a 50 μ L cuvette with a concentration of 3 μ M. The sample was then analysed *via* an HPLC with a Synergi Fusion-RP (80 \AA , 4 μ m, 150 x30 mm, Flowrate 1mL/min) to separate the two different isomers. The two diastereomers of the closed ring form also absorb light in the visible range and can therefore be differentiated from the open isomer. Integration of the corresponding peaks leads to the ratio between the open and the closed isomer. The extinction coefficients of both isomers at 260 nm are nearly the same due to the strong absorption of the nucleotides at this wavelength, which allows the integration of the peaks to extract the switching efficiency. For PS1, a switching efficiency of 50 % could be determined.

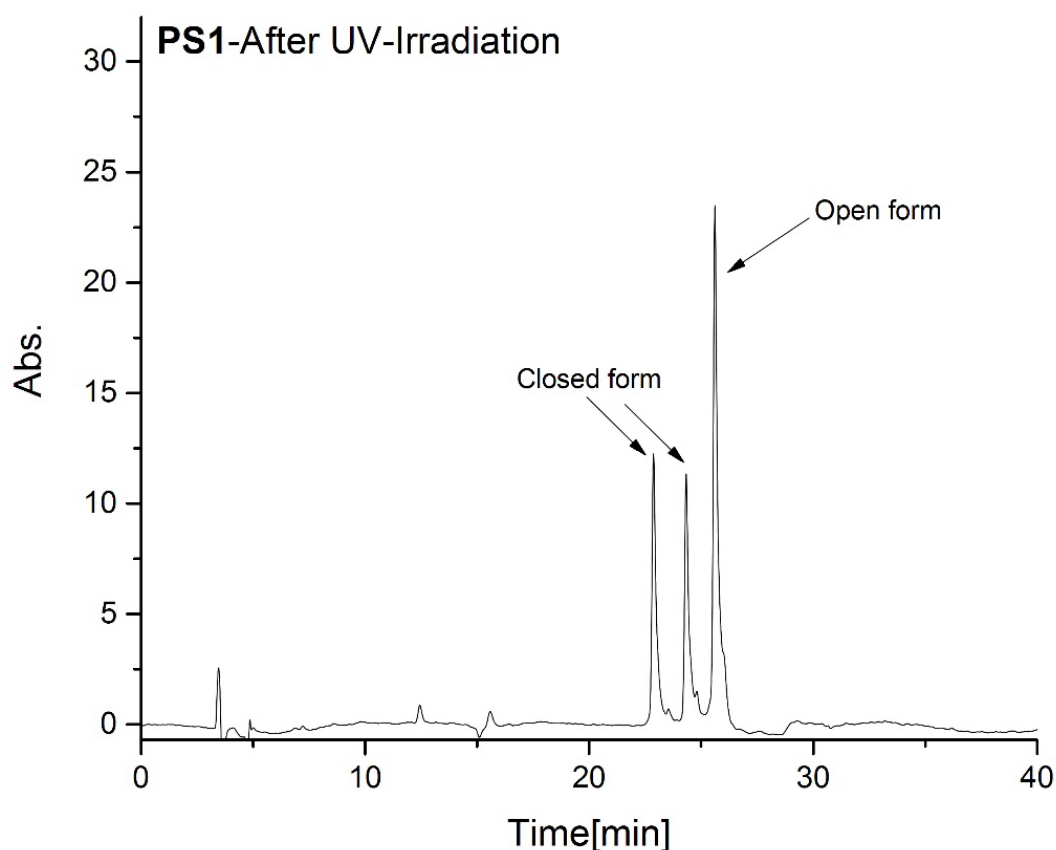


Figure S2. HPLC time trace of PS1 after 10 min of UV-irradiation with a 310 nm LED (Thorlabs M310L3) at 260 nm.

Table S2: HPLC gradient for the determination of the switching efficiency of PS1

Method D	
Time [min]	Buffer B [%]
0	7.5
10	12.5
35	40
40	50
45	100
50	100
52	7.5

S5: Absorbance of one *versus* three photochromic nucleotides.

Photochromic strands PS1 and PS3 were hybridized with the donor and acceptor strands to generate the all-optical excitonic switch in two different configurations as shown in Figures 1a and 1b of the manuscript. The expectation was that incorporation of three photochromic nucleotides would produce a three-fold increase in the donor-acceptor emission modulation. Figure S3 shows the saw-tooth plots created from the emission data collected for 5 μM (Panels a and c) and 20 μM (Panels b and d) concentrations in the liquid environment with either one (Panels a and b) or three (Panels c and d) photochromic nucleotides attached. When a single photochromic nucleotide was used (Fig. S3a & S3b), the donor and acceptor emission was compared after each opening and closing event to reveal any saw-tooth behavior indicative of modulation. For the 5 μM single photochromic nucleotide sample, modulation is initially barely visible (1.0% and 0.6%) but disappears during later cycling. However, for the 20 μM sample, a 6.6% and 5.0% saw-tooth modulation is observed. When three photochromic nucleotides were present (Figs. S3c & S3d), clear modulation of the donor and acceptor emission were observed in the 5 μM (8.2% and 7.8% respectively) and 20 μM samples (15.1% and 8.4% respectively).

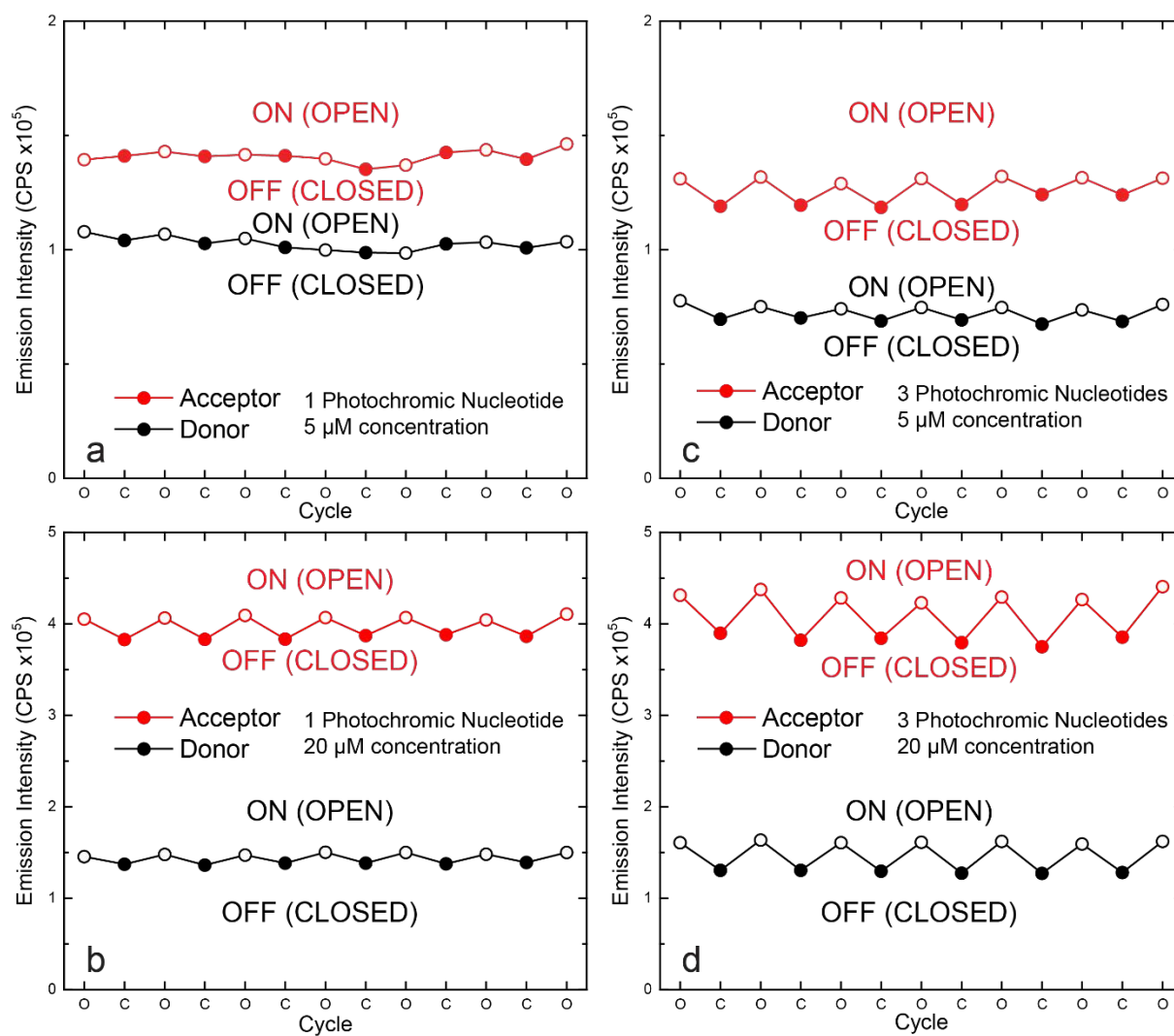


Figure S3. Saw-tooth plots of the all-optical excitonic switch operating in the liquid phase demonstrating the changes in the donor and acceptor emission as the photochromic nucleotides are cycled between the open and closed configuration (*i.e.*, ON and OFF states) six times. **(a)** 5 μ M switch with a single photochromic nucleotide (strand PS1) demonstrates minimal modulation between the ON and OFF states. **(b)** 20 μ M switch with a PS1 strand demonstrates 6.6% modulation between the ON and OFF state. The weak modulation noted in **a** may be due to the emission of the donor/acceptor pair overwhelming the single photochromic nucleotide as well as

the low absorbance of the single photochromic nucleotide. **(c)** 5 μ M switch with three photochromic nucleotides attached (PS3 strand) demonstrates 8.2% modulation between the ON and OFF states. **(d)** 20 μ M switch with a PS3 strand produces the greatest amount of donor/acceptor emission modulation (15.1%). The increased modulation results from the greater absorbance provided by the three photochromic nucleotides.

S6: Fluorescence measurements.

Optical characterization involving acquisition of both the absorbance and fluorescence spectra of the all-optical excitonic switch was performed. UV-Vis absorbance spectra were collected for each individual strand using a dual-beam Cary 5000 UV-Vis-NIR spectrophotometer (Agilent Technologies). Static and dynamic emission spectra were collected using a Fluorolog-3 spectrofluorometer (HORIBA Scientific). Fluorescence emission detector geometries are illustrated in Figure S4.

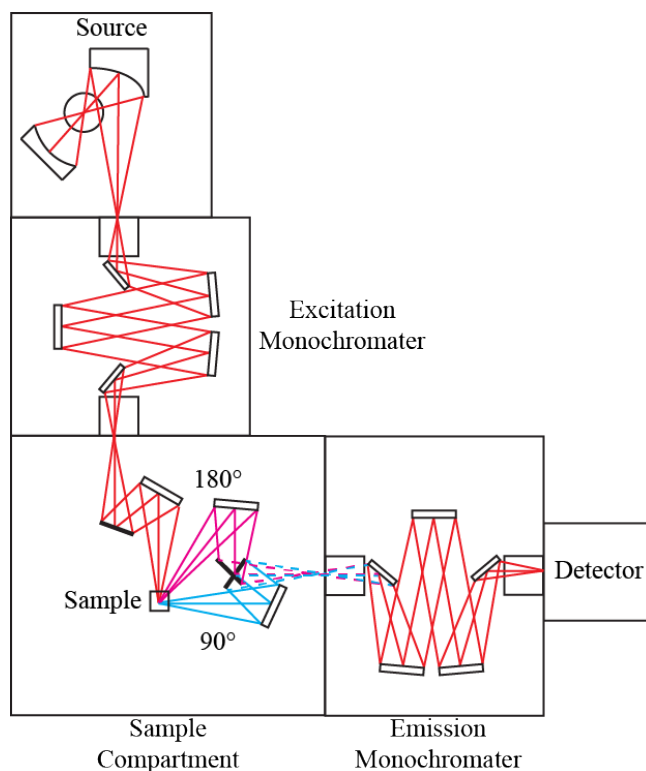


Figure S4. Detector geometry for acquisition of all-optical excitonic emission spectra. For the liquid environment measurements, a perpendicular excitation light source interacts with the sample *via* a 2 mm by 2 mm window on the source side of the cuvette. The fluorescence emission is transmitted through a 2 mm by 10 mm window on the detector side of the cuvette (cyan lines) and detected *via* a photomultiplier tube (PMT, detector) aligned at 90° relative to the excitation. For the solid environment measurements, the excitation light source remained perpendicular to the sample, but the detector samples fluorescence emission aligned ~180° relative to the sample (purple lines). The solid alignment geometry is required because very little fluorescence emission is delivered in the direction parallel to the quartz slide.

S7: Controls.

In order to better understand the interaction of the photochromic nucleotides with the donor and acceptor chromophores, a series of control experiments were performed wherein specific DNA strands of the all-optical excitonic switch were replaced with bare ssDNA strands as illustrated in Figures S5a, S5d, S5g, and S5j. When the acceptor chromophore was omitted from the all-optical excitonic switch, (Fig. S5 a-c), we hypothesized that modulation of the donor by the photochromic nucleotides *via* absorption, FRET, or both processes should occur. As shown in Figure S1, the photochromic nucleotides in the closed absorbing configuration, (red dashed curve), can interact with both the donor absorbance (blue dashed curve) and emission (blue solid curve). Figures S5b & S5c demonstrate some emission intensity modulation, indicating the photochromic nucleotides absorb excitonic energy and interrupt FRET transfer of the donor emission. We therefore conclude the saw-tooth plot shown in Figure S5c validates our excitonic energy absorption hypothesis, which in turn causes FRET transfer modulation. Likewise, when the donor dye was omitted from the all-optical excitonic switch (Fig. S5 d-f), we hypothesized that the modulation of the acceptor by the photochromic nucleotides *via* absorption, FRET, or both should occur. As shown in Figure S1, the photochromic nucleotides in the closed absorbing configuration (red dashed curve) can interact with both the acceptor absorbance (green dashed curve) and emission (green solid curve). Figures S5e & S5f demonstrate some emission intensity modulation, confirming the hypothesis that the photochromic nucleotides also absorb excitonic energy and interrupt FRET transfer to the acceptor dye. We further hypothesized no modulation would be observed for the following controls: when photochromic nucleotides were not included in the switch construct (Fig. S5g) or when both the donor and the acceptor were excluded from the switch construct (*i.e.*, only photochromic nucleotides present) and mixed in solution with a switch construct with only the

donor and acceptor (*i.e.*, no photochromic nucleotide; Fig. S5j). For the latter control (Fig. S5j), we assumed that no near field interaction, and thus no modulation, would occur between the photochromic nucleotides-only switch construct and the donor/acceptor pair-only construct (Fig. S5j). Both negative controls, Figures S5 h-i & S5 k-l, demonstrate virtually no modulation took place when cycling the all-optical excitonic switch controls, thus substantiating our hypotheses. The data shown in Figure S5i do not show saw-tooth behavior and thus suggest that modulation *via* excitonic absorption or FRET interruption is not possible without the photochromic nucleotides present. Figure S5l does not show saw-tooth behavior and this absence of modulation reinforces the need for direct, distance dependent interaction of the photochromic nucleotides with the donor/acceptor pair in order to produce excitonic absorption and FRET interruption. We note the data shown in Figure S5k do indicate some inner filter effect¹ on the donor emission in the presence of the photochromic nucleotides-only switch; this can be seen by comparing the donor emission in Figure S5h and S5k. The control experiments do indicate there are a variety of potential pathways for energy transfer, and further studies, which are beyond the scope of this paper, are warranted and could be conducted in the future.

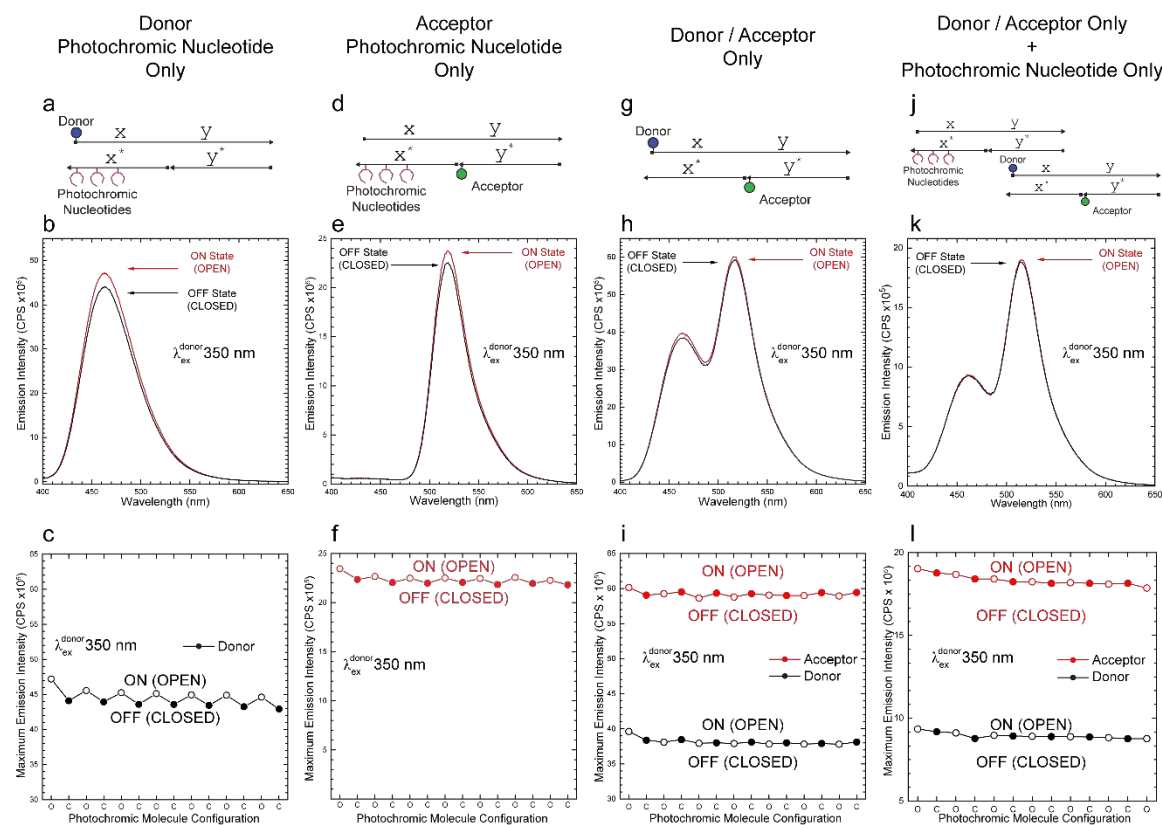


Figure S5. All-optical excitonic switch controls performed at 5 μM DNA concentration in the liquid environment. (a, b, c) Donor with three photochromic nucleotides hybridized (no acceptor present) produced slight modulation of the donor emission, indicating excitonic absorption and FRET transfer interruption. (d, e, f) Acceptor with three photochromic molecules hybridized (no donor present) produced slight acceptor emission modulation demonstrating excitonic absorption and FRET transfer interruption. (g, h, i) Donor/Acceptor with no photochromic nucleotides hybridized produced no significant modulation of either the donor or acceptor emission curve, signifying the excitonic absorption and FRET transfer interruption is directly attributable to the presence of the photochromic nucleotides. (j, k, l) Donor/Acceptor dyes hybridized plus three photochromic nucleotides hybridized to a bare all-excitonic construct outside the Förster radius produced negligible modulation. All data presented without normalization for concentration nor (in the case of k, l) for dilution.

S8: Solid phase concentration calculations

To determine the location of the all-optical excitonic switches in the solid phase sample, we collected a fluorescence optical image of the solid phase sample using a ProteinSimple FluoroChem Q MultiImage III chemiluminescent imaging system running AlphaView software version 3.4.0.0. as shown in Figure S6a. Since a 534 nm excitation filter and a 606 nm emission filter was used, only the emission of the acceptor was collected. The grayscale image was reversed in order to enhance the contrast between the sample and the quartz slide, hence the emission is shown as black. The fluorescence image shows that the all-optical excitonic switches are located only in the outer elliptical ring of the solid phase sample.

To estimate the bulk concentration of the solid phase sample, profilometry measurements were performed using a Bruker Dektax XT-A Stylus profilometer (Fig. S6b). The profilometry data were plotted (Figs. S6c & d) and the resulting radial distances and profile height along the lateral and longitudinal ellipse directions were used to calculate the volume of the ellipse and, specifically, the volume of the outer elliptical ring. Note that most of the solid phase sample, and thus the all-optical excitonic switches, reside in the outer elliptical ring which correlates with the emission image (Fig. S6a) showing the location of the all-optical excitonic switches. The data suggest that evaporation while the sample was desiccated initially occurred from the center of the sample and moved outward during the transition from the liquid to solid phase. Hence, very little of the solid phase is within the inner ellipse and is instead primarily located in the outer elliptical ring. The solid phase concentration of all-optical excitonic switches can then be determined from the volume of the solid phase in the outer elliptical ring using the following Equations (1 – 6):

$$A_i = \pi r_1 r_2 \quad (1)$$

$$A_e = \pi r_3 r_4 \quad (2)$$

where r_1 and r_2 are the radii (major and minor) of the inner portion of the ellipse, r_3 and r_4 are the radii of the entire ellipse, and A_i and A_e are the areas of the inner and entire ellipses, respectively.

The area, A_r , and volume, V_r , of the outer elliptical ring are given by:

$$A_r = A_e - A_i, \quad (3)$$

$$V_r = A_r H_r, \quad (4)$$

where H_r is the height of the outer elliptical ring. The concentration of the all-optical excitonic switches can be found using mass balance relationship:

$$C_r V_r = C_{liq} V_{liq}, \quad (5)$$

where C_r is the concentration of the all-optical excitonic switches in the outer elliptical ring while C_{liq} and V_{liq} are the concentration and volume of the liquid phase solution pipetted on the slide, respectively.

Solving for the concentration of the all-optical excitonic switches, C_r , we have:

$$C_r = \frac{C_{liq} V_{liq}}{V_r}. \quad (6)$$

Using the profilometry data, Equation 6 was used to calculate the concentration of the all-optical excitonic switches in the solid phase and is listed in Table S3.

As a frame of reference (*i.e.*, validity check) to C_r determined *via* Equation 6 using the profilometry data, a theoretical approach was also used to estimate the concentration of all-optical excitonic switches in the solid phase by using the volume of the double stranded DNA (dsDNA) scaffold, V_{dsDNA} , given by:

$$V_{dsDNA} = \pi r^2 l, \quad (7)$$

where the r and l are the radius and length of the dsDNA, respectively. The concentration of all-optical excitonic switches, $C_{r,theory}$, is determined by:

$$C_{r,theory} = \frac{1 \text{ switch mole}}{V_{dsDNA} \text{ Av \#}}, \quad (8)$$

where $Av \#$ is Avogadro's number. Equation 8 was used to calculate the theoretical concentration of all-optical excitonic switches in the solid phase and is listed in Table S3 to compare to that calculated by Equation 6. The comparison shows that the values are within an order of magnitude. Hence, the profilometry approach to determine the concentration of the all-optical excitonic switches in the solid phase is sound.

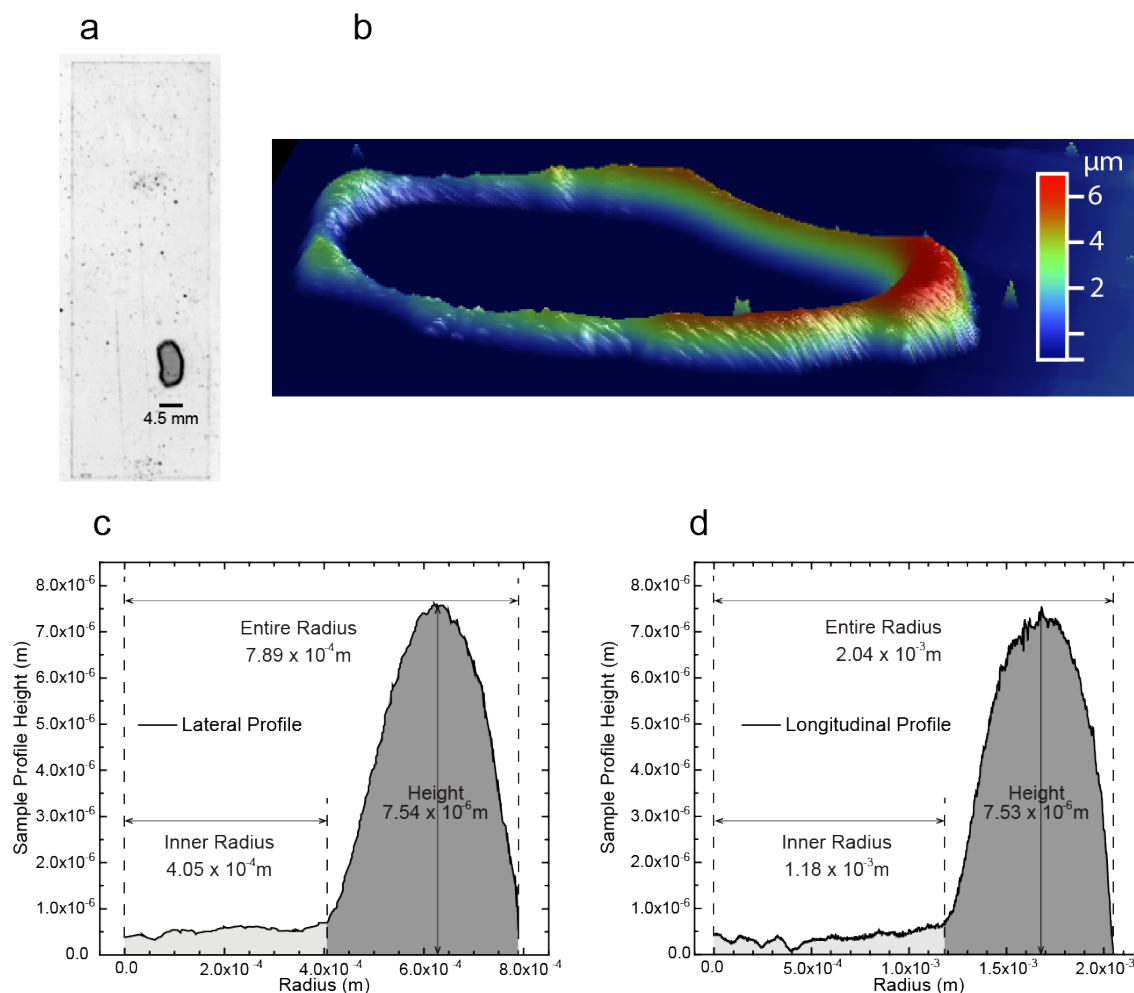


Figure S6. (a) Representative solid phase sample imaged using a 534 nm excitation filter and a 606 nm emission filter; the grayscale image was reversed for clarity. A clear elliptical ring on the outer periphery can be observed in the image indicating the all-optical excitonic switch migrates to the edges of the sample during desiccation. The elliptical ring dimensions are confined within the window size of the fluorometer excitation beam. (b) 3D profilometer map of a representative solid phase sample where the elliptical ring is observed within the outer periphery of the sample. (c & d) Profilometer data collected from the solid phase sample along the lateral and longitudinal directions of the ellipse. For each direction, the sample height and the inner and outer ellipse radii

are indicated. Note that the profiles have been divided into the non-fluorescing region (light shading) and the fluorescing region (dark shading).

Table S3: Liquid and solid phase concentration values

	Liquid Phase Volume, V_{liq} (L)	Liquid Phase Concentration, C_{liq} (M)	Solid Phase Volume, V_r (L)	Solid Phase Concentration, C_r (M)
Profilometer	5.0×10^{-6}	20×10^{-6}	8.5×10^{-9}	16×10^{-3}
Theoretical	X	X	X	52×10^{-3}

S9. Solid phase variation

A 30 nm blue shift is noted in the donor emission of the solid phase sample (Manuscript Figure 2d). A potential cause of the blue shift in the solid phase sample may be due to solvatochromic changes of the chromophores as a result of solidification from the liquid phase.²

S10: Switching time derivation:

Assuming a first order reaction rate for the all-optical switch's opening and closing upon exposure to specific wavelengths of light, the relationship between Δ_s and t_e is:

$$\Delta_s = S \left[\frac{(1 - e^{-t_e/\tau_o})(1 - e^{-t_e/\tau_c})}{1 - e^{-(\tau_o + \tau_c)t_e/\tau_o\tau_c}} \right], \quad (9)$$

where τ_o and τ_c are the mean time to modulate from closed to open, and the mean time to modulate from open to closed, respectively, and S is a single offset representative of the steady state equilibrium (see S11 for complete derivation). The simple elegance of Equation 9 allows Δ_s *versus* t_e data to be modeled with a single parameter, S . The validity of the hypothesis is then tested by modeling Δ_s *versus* t_e data using Equation 9.

Obtained from the static emission scans, Δ_s of the donor or acceptor is defined as the fractional difference between the maximum emission intensities in the ON or OFF state of either the donor or the acceptor, and is given by:

$$\Delta_s = \frac{I_{open} - I_{close}}{I_{open}}, \quad (10)$$

where I_{open} and I_{closed} are the maximum donor (462 nm liquid and 433 nm solid) or acceptor (517 nm liquid and 513 solid) emission intensities when the photochromic nucleotides are in the open configuration or closed configuration, respectively. For each exposure time, Δ_s was determined and plotted as a function of the state (ON *versus* OFF) as shown in Figure 3a.

Assuming first order reaction kinetics behavior for ring opening and closing of the photochromic nucleotides,³ the dynamic modulation emission data (Figs. 2c & f) can be fit with an exponential function described by:

$$I = I_o e^{-t_e/\tau_i} + I_{offset}, \quad (11)$$

where I , I_o , t_e , and τ_i are the final emission intensity of the donor or acceptor, the initial emission intensity of the donor or acceptor, the photochromic nucleotides' exposure time, and the mean time for modulation (time to open, $\tau_i=\tau_o$, or close, $\tau_i=\tau_c$, the photochromic nucleotides), respectively. I_{offset} establishes the donor or acceptor emission intensity offset from a zero baseline. From Equation 11, values for τ_i may be extracted for both the closed to open cycle (τ_o) and open to closed cycle (τ_c), and their sum (τ_Σ) should theoretically be the same as t_s , the characteristic switching time shown below.

The data in Figure 2 of the manuscript were obtained with a t_e of 30 seconds; therefore, only one t_e can be used in Equation 11. To determine the validity of our hypothesis (*i.e.*, Equation 9), a set of time trial experiments were necessary and therefore performed over a range of specifically chosen t_e 's for the photochromic nucleotides and t_s was thereby obtained. For each t_e of the time trials experiments, saw-tooth plots were generated as shown in Figure 3a and 3d of the manuscript, and Δ_s of the donor and the acceptor emission were calculated using Equation 10.

Equation 11 was used to fit the dynamic modulation data from each of the time trial experiments. Manuscript Figure 3b and 3e shows the fits of the averaged (6 data sets) dynamic modulation data for a photochromic nucleotide t_e of 30 seconds for both the liquid and solid phase, respectively. Both τ_o and τ_c were extracted from the liquid and the solid phase averaged dynamic modulation

data. A τ_o value of 5.7 ± 0.4 (standard deviation) and 11.8 ± 5.1 seconds was given for the liquid and solid phase, respectively, and a τ_c value of 8.4 ± 0.5 and 8.1 ± 2.8 seconds was given for the liquid and solid phase, respectively (see Table S4 for all time trial data). The complete time to cycle between the open and closed state (τ_Σ) is 14.1 ± 0.9 seconds for the liquid phase and 19.9 ± 7.8 seconds for the solid phase. Figures 3b and 3e are representatives of all time trial dynamic modulation data collected.

S11. Characteristic switching time derivation

General equations

Here we obtain an expression for the switching amplitude as a function of time for the all-optical excitonic switch.

Let $[O]$ denote the concentration of open photochromic nucleotides and let $[C]$ denote the concentration of closed photochromic nucleotides, then:

$$[O] + [C] = [S], \quad (12)$$

where $[S]$ is the total concentration of photochromic nucleotides.

Let I_o denote the photon flux of the light source used to open the photochromic nucleotides and let σ_o be the absorbance cross-sectional area for photochromic nucleotides opening. Then, the equation for the rate with which closed photochromic nucleotides are being lost from the sample due to conversion into open photochromic nucleotides is:

$$\frac{d[C]}{dt} = -\sigma_o I_o [C]. \quad (13)$$

Similarly, let I_c be the photon flux of the light source used to close the photochromic nucleotides and let σ_c be the absorbance cross-sectional area for photochromic nucleotides closing. The rate with which the open photochromic nucleotides are being removed from the sample by conversion into closed photochromic nucleotides is:

$$\frac{d[O]}{dt} = -\sigma_c I_c [O]. \quad (14)$$

It is useful to introduce the switching rates (γ_i) and switching times (t_i) for opening ($i = o$) and closing ($i = c$) the photochromic nucleotides according to:

$$\gamma_o = \frac{1}{t_o} = \sigma_o I_o, \quad (15)$$

and

$$\gamma_c = \frac{1}{t_c} = \sigma_c I_c. \quad (16)$$

Switching equations

We consider the case when the all-optical excitonic switch is being cycled back and forth between the open and closed configuration. Consider a sequence of exposure times t_n labeled by successive integers n , where $n = 0, 1, 2, 3, \dots$, at which cycling from one configuration to the other is initiated. During the times t for which $t_{2n} < t < t_{2n+1}$ the photochromic nucleotides are being exposed with light that opens the photochromic nucleotides. Hence, from Equations (13) and (15) one has:

$$\frac{d[C]}{dt} = -\gamma_o [C], \text{ when } t_{2n} < t < t_{2n+1}. \quad (17)$$

During the times t for which $t_{2n+1} < t < t_{2n+2}$, the photochromic nucleotides are being exposed with light that closes the photochromic nucleotides. Hence, from Equations (14) and (16), one obtains:

$$\frac{d[O]}{dt} = -\gamma_c [O], \text{ when } t_{2n+1} < t < t_{2n+2}. \quad (18)$$

Integrating Equation (17) within the exposure time interval $t_{2n} < t < t_{2n+1}$ gives:

$$[C] = [C]_{t_{2n}} e^{-\gamma_o(t-t_{2n})}, \text{ for } t_{2n} < t < t_{2n+1}. \quad (19)$$

Integrating Equation (18) within the exposure time interval $t_{2n+1} < t < t_{2n+2}$ gives:

$$[O] = [O]_{t_{2n+1}} e^{-\gamma_c(t-t_{2n+1})}, \text{ for } t_{2n+1} < t < t_{2n+2}. \quad (20)$$

Evaluating the concentrations at the end of the exposure time intervals, Equations (19) and (20) yield:

$$[C]_{t_{2n+1}} = [C]_{t_{2n}} e^{-\gamma_o(t_{2n+1}-t_{2n})}, \quad (21)$$

$$[O]_{t_{2n+2}} = [O]_{t_{2n+1}} e^{-\gamma_c(t_{2n+2}-t_{2n+1})}. \quad (22)$$

We now take all the exposure time intervals to be the same, that is:

$$t_{n+1} - t_n = t_e \text{ for all } n. \quad (23)$$

Hence, Equations (21) and (22) become:

$$[C]_{t_{2n+1}} = [C]_{t_{2n}} e^{-\gamma_o t_e}, \quad (24)$$

$$[O]_{t_{2n+2}} = [O]_{t_{2n+1}} e^{-\gamma_c t_e}. \quad (25)$$

Using Equation (12), this last equation yields:

$$[S] - [C]_{t_{2n+2}} = ([S] - [C]_{t_{2n+1}}) e^{-\gamma_c t_e}. \quad (26)$$

This can be rearranged to give:

$$[C]_{t_{2n+2}} = [S](1 - e^{-\gamma_c t_e}) + [C]_{t_{2n+1}} e^{-\gamma_c t_e}. \quad (27)$$

Using Equation (21) this becomes:

$$[C]_{t_{2n+2}} = [S](1 - e^{-\gamma_c t_e}) + [C]_{t_{2n}} e^{-(\gamma_o + \gamma_c) t_e}. \quad (28)$$

When cycling back and forth for over a long period of time, steady state is achieved in which:

$$[C]_{t_{2n+2}} = [C]_{t_n}, \text{ for all } n, \quad (29)$$

and similarly for the $[O]$ concentration. Hence, Equation (28) becomes:

$$[C]_{t_{2n}} = [S](1 - e^{-\gamma_c t_e}) + [C]_{t_{2n}} e^{-(\gamma_o + \gamma_c) t_e}. \quad (30)$$

Solving this equation for $[C]_{t_{2n}}$ yields the steady-state value:

$$[C]_{t_{2n}} = [S] \frac{1 - e^{-\gamma_c t_e}}{1 - e^{-(\gamma_o + \gamma_c) t_e}}. \quad (31)$$

Substituting Equation (31) into Equation (24) yields the following expression for the steady state value of $[C]_{t_{2n+1}}$:

$$[C]_{t_{2n+1}} = [S] \frac{e^{-\gamma_o t_e} (1 - e^{-\gamma_c t_e})}{1 - e^{-(\gamma_o + \gamma_c) t_e}}. \quad (32)$$

The switching amplitude Δ_s is the difference, as measured by emission, between the concentration of closed photochromic nucleotides with respect to the former exposure time and the most recent exposure time given by:

$$\Delta_s = [C]_{t_{2n}} - [C]_{t_{2n+1}}. \quad (33)$$

Substituting Equations (31) and (32) into Equation (33) gives:

$$\Delta_s = [S] \frac{(1 - e^{-\gamma_o t_e})(1 - e^{-\gamma_c t_e})}{1 - e^{-(\gamma_o + \gamma_c) t_e}}. \quad (34)$$

In terms of the exposure times, Equation (34) can be written as

$$\Delta_s = [S] \frac{(1 - e^{-t_e/t_o})(1 - e^{-t_e/t_c})}{1 - e^{-(t_o + t_c)t_e/t_o t_c}}. \quad (35)$$

In the limit of very large exposure times, t_e , Δ_s no longer changes because it can be assumed that all photochromic nucleotides are either in the closed or open configuration. Hence, can be written as:

$$\lim_{\Delta t \rightarrow \infty} \Delta_s = [S], \quad (36)$$

that is, if the exposure time is long enough, all the photochromic nucleotides are cycled from one configuration to the other. Taylor expanding Equation (34) for small t_e , one has, to linear order:

$$\Delta_s = \frac{\gamma_o \gamma_c}{\gamma_o + \gamma_c} [S] t_e, \quad (37)$$

or, substituting Equations (15) and (16), gives:

$$\Delta_s = \frac{1}{t_o + t_c} [S] t_e. \quad (38)$$

At the point in which the limit of long exposure times first holds, that is, Δ_s first becomes constant (does not vary) and Equation (36) holds, then Equation (35) and Equation (36) must be equivalent hence:

$$\frac{1}{t_o + t_c} [S]_{t_e} = [S]. \quad (39)$$

The particular t_e at which Δ_s first becomes constant is defined as the characteristic switching time, t_s . Thus, Equation (39) should be written as:

$$\frac{1}{t_o + t_c} [S]_{t_s} = [S]. \quad (40)$$

In order for Equation (38) and Equation (36) to be equivalent, t_s and the sum of t_o and t_c (*i.e.*, τ_Σ) must be the same. That is:

$$t_s = \frac{\gamma_o + \gamma_c}{\gamma_o \gamma_c} = t_o + t_c = \tau_\Sigma. \quad (41)$$

The value of t_s can be determined from a plot of Δ_s *versus* t_e data in the following approach. The point of intersection between a vertical line, drawn from the x-axis, and Δ_s *versus* t_e data at the time at which Δ_s first shows non-varying, or constant, behavior provides the value of t_s . This approach is shown in Figure 3C and 3F of the manuscript.

S12: Time trial design

For the time trial experiments, the photochromic nucleotides were exposed for cycle times (t) of 1 second, 3 seconds, 5 seconds, 10 seconds, 30 seconds, 100 seconds, 300 seconds, and 1000 seconds (Table S3). Each cycle of the time trial was performed as a series of four sequential excitation/emission scans whereby *i*) the all-optical excitonic switch was initially set to the ON state and a static emission scan (400 nm to 650 nm) was collected while exciting the donor of the all-optical excitonic switch with 350 nm VIS light, *ii*) the photochromic nucleotides were exposed to 300 nm UV light (τ_c) while simultaneously collecting donor emission (460 nm), *iii*) a static emission scan (400 nm to 650 nm) was collected while exciting the donor of the all-optical excitonic switch with 350 nm VIS light, and *iv*) the photochromic nucleotides were exposed to 455 nm VIS light (τ_o) while simultaneously collecting acceptor emission (520 nm). Note that fitting of very short time scales (1, 3, and 5 seconds) is questionable due to the difficulty of fitting segments too short to observe curvature.

Table S4. Summed exposure times (τ_{Σ}) for time trial experiments conducted with the all-optical excitonic switch. One complete cycle ($t_o + t_c$) is given as τ_{Σ} and the average time of all values with the standard deviations are included.

		5 sec	10 sec	30 sec	100 sec	300 sec	1000 sec	Averaged time (sec)	Standard Deviation
LIQUID 20 μ M	t_o	5.44	5.07	5.68	5.93	6.14	5.75	5.67	± 0.37
	t_c	7.49	8.01	8.84	8.62	8.77	8.46	8.37	± 0.52
	τ_{Σ}	12.93	13.08	14.52	14.55	14.91	14.21	14.04	± 0.83
SOLID 69 mM	t_o	1.90	10.89	13.97	14.43	14.40	15.06	11.77	± 5.06
	t_c	2.84	7.44	9.47	9.49	9.67	9.96	8.14	± 2.75
	τ_{Σ}	4.74	18.32	23.45	23.92	24.07	25.02	19.92	± 7.81

S13: Absorbance cross section

The absorbance cross-section (σ) of the all-optical excitonic switch may be calculated by using the photon flux (J) determined in the previous section and the extracted mean times for modulation shown in Table S6 as follows. Let P denote the probability that a given photochromic nucleotide is switched. The time rate of change of P is given by:

$$\frac{dP}{dt} = \sigma J (1 - P). \quad (42)$$

The general solution to this differential equation is:

$$P = 1 - \exp^{-(\sigma J t)}. \quad (43)$$

Using the boundary conditions, the initial condition is $P = 0$ at ($t = 0$), and the final condition is $P = 1$ at ($t = \infty$). For the final condition, it is assumed that, if one waits long enough, all the photochromic nucleotides will have switched. Let $t_{(1/2)}$ denote the exposure time needed to cause half the photochromic nucleotides to cycle; at this time $P = 1/2$. Substituting these two quantities in Equation (43) and solving for σ , one has:

$$\sigma = \frac{\ln(2)}{J t_{(1/2)}}. \quad (44)$$

S14: Photon energy, photon fluence, and photon flux

Photon energy (E) was calculated for the two wavelengths utilized to cycle the configuration of the photochromic nucleotide using:

$$E = \frac{hc}{\lambda}, \quad (45)$$

where h is Planck's constant, c is the speed of light, and λ is the wavelength of interest. For this work, 300 nm light was used to switch the photochromic nucleotide between the open (ON) to closed (OFF) configuration (**o-c**) and 455 nm light was used to switch the photochromic nucleotide between the closed (OFF) to open (ON) configuration (**c-o**). Using Equation 45, the photon energy at 300 nm (**o-c**) is 6.62×10^{-19} Joules and at 455 nm (**c-o**) is 4.37×10^{-19} Joules.

The number of photons per second (photon fluence) is calculated with:

$$H = \frac{W}{E}, \quad (46)$$

where H is the photon fluence, W is the measured power and E is photon energy at 300 nm or 455 nm respectively. Power data collected from the Fluorolog-3 spectrofluorometer using a LABMAX_TOP (Coherent Inc.) power meter (Model 1104622) coupled to a silicon diode photodetector (PM 30) was found to be 60×10^{-6} W at 300 nm and 150×10^{-6} W at 455 nm. Using Equation 46 the photon fluence is 9.1×10^{13} photons/sec at 300 nm and 3.4×10^{14} photons/sec at 455 nm.

The photon flux (J) (photons per unit area per second) is calculated with:

$$J = \frac{W}{EA}, \quad (47)$$

where A is the spot size area. Using a spot size of $\sim 4 \text{ mm}^2$ Equation 47 yields a photon flux of 2.3×10^{19} photons/($\text{m}^2 \cdot \text{s}$) at 300 nm and 8.6×10^{19} photons/($\text{m}^2 \cdot \text{s}$) at 455 nm respectively.

S15: Ultrafast laser switching

Assuming use of a typical UV-VIS optical parametric amplifier (OPA) pumped by a 1 kHz regenerative amplified ultrafast Ti:sapphire laser (outputting sub 100 fs pulses) we can calculate the photon flux using:

$$\frac{J}{pulse} = \frac{E\lambda}{hcA}, \quad (48)$$

where E is the energy per pulse, λ is the wavelength of light to cycle the photochromic nucleotide, h is Planck's constant, c is the speed of light, and A is the spot size. Assuming 10 μ J/pulse with a beam radius of 100 μ m at the focused spot size area, Equation 48 yields a photon flux per pulse of 4.8×10^{20} photons/m² at 300 nm and 7.3×10^{20} photons/m² at 455 nm.

In order to determine the possibility of ultrafast switching of the photochromic nucleotide, we compared the photon flux produced by the Fluorolog-3 (see S13) in 30 seconds (see Figure 3c & 3f of manuscript) to the photon flux produced by a sub 100 fs pulse produced by a typical ultrafast laser system. Using Equation 47, the Horiba produces a photon flux of 6.8×10^{20} photons/m² in 30 seconds at 300 nm, whereas Equation 48 yielded a photon flux of 4.8×10^{20} photons/m² per pulse. This indicates the photon flux due to a single pulse from a typical ultrafast laser system should be sufficient to cycle the all-optical excitonic switch in the picosecond regime, with switching times limited by the intrinsic switching time of the photoswitch molecules rather than the ultrafast laser pulse duration.

S16: Comparison of the all-optical excitonic switch to a 14 nm node FinFET

Although a direct comparison of the size and speed of our all-optical excitonic switch to a state-of-the-art (SOTA) MOSFET is arguably not directly possible, a simple comparison provides some insight into physical parameters of interest. Here, the SOTA MOSFET used in the comparison is a bulk 14 nm technology node FinFET that appears to be used in Intel's 14 nm technology node computer processing units (CPUs)⁴, which includes Intel's cutting-edge Broadwell, Skylake, and Kaby Lake CPUs. While Intel uses a three-FinFET configuration in their 14 nm technology node, we will only compare one FinFET and neglect gate pitch for simplicity. With these assumptions, the FinFET parameters calculated here can be considered lower bounds. Parameters for the bulk 14 nm technology FinFET are shown in Table S4⁴⁻⁷.

Both the power and energy of the FinFET can be estimated using the simple relationship^{5,7},

$$P = C_{load} V_{dd}^2 f + I_{leak} V_{dd}, \quad (49)$$

$$E = P/f, \quad (50)$$

where P , E , C_{load} , V_{dd} , f , and I_{leak} denote power, energy, load capacitance, supply voltage, operation frequency, and leakage current of a transistor, respectively. If we assume that I_{leak} is low (not necessarily the case, but this favors the FinFET in the comparison), we can ignore the $I_{leak}V_{dd}$ term and Equation 49 becomes:

$$P = C_{load} V_{dd}^2 f. \quad (51)$$

We can approximate the C_{load} as the capacitance, C_{inv} , when the finFET is in inversion:

$$C_{load} \sim C_{inv} = \frac{L_g W_{fin} \epsilon_0 k_{ox}}{EOT + t_Q}, \quad (52)$$

where L_g , W_{fin} , ϵ_0 , k_{ox} , EOT , and t_Q are the gate length, fin width, permittivity of free space, high-k dielectric constant (HfO₂), effective oxide thickness and quantum mechanical inversion layer thickness⁸, respectively. EOT is given by:

$$EOT = t_{IL} + \frac{k_{IL}}{k_{HK}} t_{HK}. \quad (53)$$

where t_{IL} , t_{HK} , k_{IL} , and k_{HK} are the interfacial SiO₂ layer thickness, the interfacial SiO₂ layer relative dielectric constant, and the relative dielectric constant of the HfO₂, respectively. Using Equation 51, we can write the energy as:

$$E = C_{load} V_{dd}^2. \quad (54)$$

For a FinFET, we can now calculate the values of C_{load} , E , and the energy for a full cycle (*i.e.*, 2 E), which we define as ON-OFF-ON (see next paragraph). The values used for these calculations are listed in Table S4.

Table S5: Bulk Low Power 14 nm technology node FinFET parameters (after⁶)

Gate Length (L_g):	14 nm
Fin Width (W_{fin}):	10 nm
Fin Height (H_F):	100 nm
Field oxide Height (H_{FO}):	300 nm
SiO ₂ Interfacial Layer Relative Dielectric Constant (k_{IL}):	3.9
High-k Gate Oxide Thickness (t_{HK}):	~1.25 – 2.2 nm (used 1.5 nm) calculation
HfO ₂ Relative Dielectric Constant (k_{HK}):	25
Interfacial SiO ₂ layer thickness (t_{IL})	~1 nm
Quantum Mechanical Inversion Layer Thickness (t_Q)	0.3-0.4 nm (used 0.4 nm)
Source or Drain Contact Pad Area Regions ($A_{s,d}$):	$L_{s,d} \times L_{s,d} = 40 \times 40 \text{ nm}^2$
Source/Drain Contact Pad Area Regions - Distance from Gate (SD_g):	15 nm
Distance from Source to Drain (SD_d):	$L_g + 2 \times SD_g = 44 \text{ nm}$
Distance from End of Source to End of Drain (SD_{tot}):	$SD_d + 2 \times L_{s,d} = 124 \text{ nm}$
FinFET Footprint (A_{FET})	$L_{s,d} \times SD_{tot} = 496 \text{ nm}^2$
FinFET Volume (V_{FET})	$A_{FET} \times H_F = 49,600 \text{ nm}^3$
Drain or power supply voltage (V_{dd}):	~0.7 – 1.2 V (used 0.7V in calculation)
Simulated Ring Oscilator Initial Cycle time ⁹	10s of ps
$C_{FinFET} \sim C_{inv}$ (Equation 52)	0.059 fF
Energy/Cycle (Equation 54)	58 aJ

Though this approach is simplistic, the minimum energy requirements for switching the all-optical excitonic switch can be estimated using Equation 45 (Supporting Information S13) and multiplying the resultant photon energy values by the number of photochromic nucleotides present. For our device construct with three diarylethenes per photochromic nucleotide strand, the energy required to switch from the ON state to the OFF state (*i.e.*, the open configuration to the closed configuration) is 1.98 aJ (*i.e.*, 3 times the 0.66 aJ energy of a single 300 nm photon). The energy required for the reverse process (*i.e.*, OFF to ON state or closed to open configuration) is less, 1.32 aJ, due to the lower energy per photon of the 455 nm photons used. Thus, the total energy consumed in one full switching cycle (*i.e.*, ON-OFF-ON or OFF-ON-OFF) is 3.3 aJ. Full parameters for the all-optical excitonic switch are shown in Table S5. Times to open and close the diarylethene photochromic nucleotide are taken from references^{10, 11}.

Table S6: Parameters for All-Optical Excitonic Switch

Length (L):	$\sim 20 \text{ bp} \times 0.34 \text{ nm} = 6.8 \text{ nm}$
Width (W):	2 nm
Height (H):	2 nm + 1 nm = 3 nm
Footprint Area (A):	$L \times W = 13.6 \text{ nm}^2$
Volume (V):	$A \times H = 40.8 \text{ nm}^3$
Diarylethene decay time (t_d)	4 – 40 ps
Diarylethene open time (t_o)	40 ps
Diarylethene close time (t_c)	4 ps
Cycle time (t_c)	$t_o + t_c = 44 \text{ ps}$
Energy/Cycle	3.3 aJ

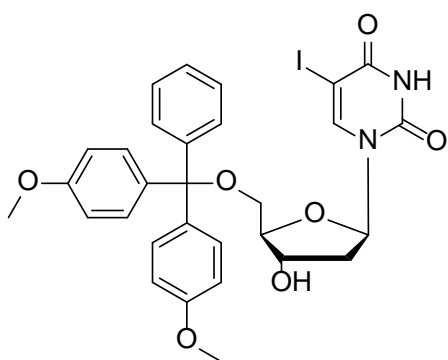
The energy to flip the FinFET to the ON state (*i.e.*, into strong inversion), using equation 54, was determined to be ~ 29 aJ. The energy to flip the FinFET to the OFF state is assumed to be the same, hence the energy per cycle (*i.e.*, flipping from OFF to ON to OFF states) was calculated to be 58 aJ. Note that this energy/cycle is a lower bound since the energy due to the leakage current in the OFF state is ignored (see equations 49 and 50 and accompanying assumptions). Comparisons between similar parameters for the FinFET (Table S4) and the all-optical excitonic switch (Table S5) reveal that the all-optical switch's footprint is 37x more compact, volume is over 3 orders of magnitude smaller, and energy consumption is over an order of magnitude less than that of the 14 nm FinFET. While it is difficult to find directly measured finFET cycle times, simulations show 14 nm FinFET ring oscillator initial cycle times in the 10s of ps and simulated write times to 6-finFET static random access memory (SRAM) in the 1s to 10s of ps, but do not discuss read times.⁹

¹² It is reasonable to assume that cycle times for a single finFET is in the 10s of ps which is certainly comparable to or better than the photoisomerization reaction cycle times for diarylethene molecules. Although the calculations we have employed are simple first order approximations that one can argue should not be used as direct comparisons, they are rather compelling and do allude to the potential capabilities and impact of the all-optical excitonic switch for both low power and

high speed applications relative to the current semiconductor electronics state of the art. Finally, in addition to the lower energy required per switching cycle for the all-optical excitonic switch calculated in the above comparison, it should be noted that the FinFET supply voltage, V_{dd} , is always applied, whereas once the all optical excitonic switch is in a given state (ON or OFF), the state is stable and thus no additional energy is required to maintain that state.

S17: Photochromic nucleotide synthesis, attachment, and purification

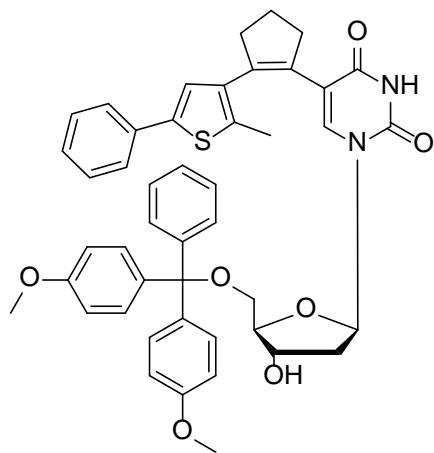
1-((2R,4S,5R)-5-((bis(4-methoxyphenyl)(phenyl)methoxy)methyl)-4-hydroxytetrahydrofuran-2-yl)-5-iodopyrimidine-2,4(1H,3H)-dione (1)



In a Schlenk flask under argon 5-iodo-2'-deoxy-uridine (5 g, 14.12 mmol) was dissolved in dry pyridine (80 mL). 4,4-Dimethoxytritylchloride (DMT-Cl) (5.76 g, 17.01 mmol) was added and the mixture stirred overnight at room temperature. Ice water was added and the reaction mixture extracted with dichloromethane (DCM). The combined organic phases were washed with water and brine, dried over MgSO₄, filtered, and the solvent removed under reduced pressure. Purification by flash column chromatography (silica gel, DCM/MeOH 50:1 + 1% NEt₃) afforded **1** as a white solid with a yield of 85% (7.9 g, 12.0 mmol).

¹H NMR (300 MHz, methanol-*d*₄): δ = 8.20 (s, 1H), 7.51 – 7.18 (m, 9H), 6.93 – 6.83 (m, 4H), 6.23 (dd, *J* = 7.5, 6.0 Hz, 1H), 4.48 (dt, *J* = 5.8, 2.9 Hz, 1H), 4.05 (q, *J* = 3.2 Hz, 1H), 3.79 (s, 6H), 3.36 (d, *J* = 3.3 Hz, 2H), 2.46 – 2.27 (m, 2H).

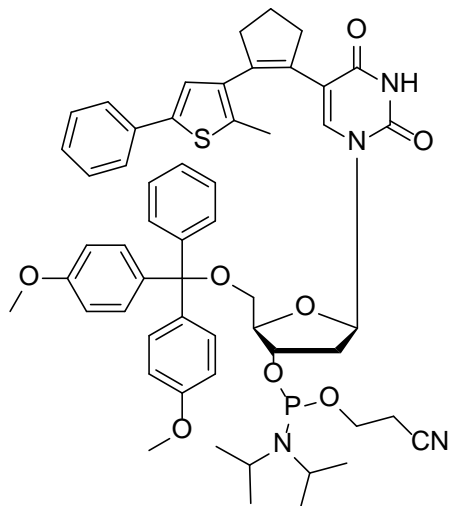
1-((2*R*,4*S*,5*R*)-5-((bis(4-methoxyphenyl)(phenyl)methoxy)methyl)-4-hydroxytetrahydrofuran-2-yl)-5-(2-(2-methyl-5-phenylthiophen-3-yl)cyclopent-1-en-1-yl)pyrimidine-2,4(1*H*,3*H*)-dione (2)



In a microwave vial **1** (100 mg, 0.15 mmol), 4,4,5,5-tetramethyl-2-(2-(2-methyl-5-phenylthiophen-3-yl)cyclopent-1-enyl)-1,3,2-dioxaborolane, (110 mg, 0.31 mmol), Pd(dppf)Cl₂ (7 mg, 8 μmol), and Cs₂CO₃ (250 mg, 0.8 mmol) were dissolved in acetonitrile (2 mL) and water (1 mL) under argon. The mixture was degassed 3 times, the vial sealed, and stirred at 120°C for 1 hr. The reaction mixture was absorbed on silica and purified by flash column chromatography (silica gel, DCM/MeOH 20:1 + 1% NEt₃), affording **2** as yellowish solid in a yield of 90% (104 mg, 0.13 mmol).

¹H NMR (300 MHz, methanol-*d*₄): δ = 7.60 – 7.18 (m, 14H), 7.11 (s, 1H), 6.88 – 6.77 (m, 4H), 6.70 (s, 1H), 6.18 (t, *J* = 6.6 Hz, 1H), 3.86 (dt, *J* = 7.4, 3.7 Hz, 1H), 3.80 (s, 3H), 3.75 (s, 3H), 3.63 (dt, *J* = 7.7, 4.0 Hz, 1H), 3.04 (ddd, *J* = 24.9, 10.2, 3.1 Hz, 2H), 2.84 (dt, *J* = 14.0, 7.2 Hz, 1H), 2.60 (dt, *J* = 14.8, 7.4 Hz, 2H), 2.16 – 2.08 (m, 1H), 2.07 (s, 3H), 2.05-2.00 (m, 1H), 1.57 (dt, *J* = 13.9, 7.1 Hz, 2H). ¹³C NMR (125 MHz, methanol-*d*₄): δ = 164.60, 160.15, 151.50, 146.24, 142.03, 138.94, 137.96, 137.30, 137.24, 136.74, 135.32, 134.58, 134.48, 133.37, 131.41, 131.21, 130.07, 129.34, 128.87, 128.43, 127.82, 126.28, 125.20, 114.21, 114.13, 113.14, 87.48, 87.16, 85.56, 75.83, 72.11, 65.70, 55.77, 41.49, 38.86, 25.03, 23.64, 14.12. HRMS (ESI, positive) *m/z*: [M+Na]⁺ calc. for [C₄₆H₄₄N₂O₇SNa]⁺: 791.2761, found: 791.2725.

(2*R*,3*R*,5*R*)-2-((bis(4-methoxyphenyl)(phenyl)methoxy)methyl)-5-(5-(2-(2,5-dimethylthiophen-3-yl)cyclopent-1-en-1-yl)-2,4-dioxo-3,4-dihydropyrimidin-1(2*H*)-yl)tetrahydrofuran-3-yl(2-cyanoethyl) diisopropylphosphoramidite (**3**)



In a Schlenk flask under argon **2** (520 mg, 0.68 mmol) and Hünig's base (0.18 mL, 1 mmol) were dissolved in dry DCM (10 mL) and cooled down to 0°C. 2-cyanoethyl *N,N*-diisopropylchlorophosphoramidite (CEP-Cl, 0.31 mL, 1.1 mmol) was added, and the mixture was stirred at room temperature for 3 hrs. Purification *via* flash column chromatography (silica gel, DCM/MeOH 100:1 + 1% NEt₃) afforded **3** as a white solid with a yield of 84% (550 mg, 0.57 mmol) as a mixture of isomers.

¹H NMR (500 MHz, CDCl₃): δ = 7.42 – 7.36 (m, 2H), 7.26 (s, 11H), 7.01 (d, *J* = 1.2 Hz, 1H), 6.79 (ddd, *J* = 8.8, 6.8, 2.0 Hz, 4H), 6.69 (d, *J* = 3.3 Hz, 1H), 6.18 (ddd, *J* = 7.8, 5.7, 1.9 Hz, 1H), 4.25 – 4.08 (m, 1H), 4.07 – 4.01 (m, 1H), 3.97 (tt, *J* = 6.8, 3.9 Hz, 1H), 3.95 – 3.84 (m, 2H), 3.79 (dd, *J* = 6.0, 4.7 Hz, 5H), 3.68 – 3.39 (m, 6H), 3.11 (dtd, *J* = 10.6, 6.5, 3.1 Hz, 2H), 3.01 (tt, *J* = 11.1, 5.6 Hz, 2H), 2.83 – 2.70 (m, 2H), 2.71 – 2.53 (m, 4H), 2.46 (t, *J* = 6.5 Hz, 1H), 2.30 – 2.18 (m, 2H), 2.08 – 2.01 (m, 4H), 1.50 – 1.41 (m, 1H), 1.38 (d, *J* = 13.8 Hz, 3H), 1.33 (t, *J* = 7.4 Hz, 1H), 1.29 – 1.21 (m, 8H), 1.20 – 1.14 (m, 4H), 1.11 (dd, *J* = 11.6, 6.8 Hz, 5H), 1.04 (d, *J* = 6.8 Hz, 3H), 0.92 (d, *J* = 6.8 Hz, 3H). ¹³C NMR (125 MHz, CDCl₃): δ = 161.64, 158.76, 158.65, 149.50, 149.49, 144.61, 144.61, 140.73, 140.69, 137.49, 137.43, 137.11, 137.09, 136.23, 136.22, 135.50, 135.49, 134.20, 134.16, 133.63, 133.51, 133.00, 132.97, 130.45, 130.38, 130.08, 130.03, 129.08, 128.40, 128.34, 128.05, 128.04, 127.38, 127.36, 127.03, 126.99, 125.45, 125.39, 124.20, 124.14, 117.54, 117.46, 117.01, 113.31, 113.29, 112.43, 112.42, 110.16, 86.47, 86.46, 85.24, 85.21, 85.03, 84.98, 84.23, 84.20, 77.16, 73.78, 73.65, 73.46, 73.32, 64.11, 64.02, 64.01, 58.42, 58.40, 58.31, 58.27, 58.25, 55.42, 55.40, 55.37, 45.50, 45.45, 43.44, 43.36, 43.34, 43.26, 39.34, 38.13, 36.05, 36.03, 25.39, 25.37, 25.04, 25.03, 24.97, 24.72, 24.69, 24.66, 24.64, 24.59, 24.54, 24.53, 24.48, 23.15, 23.13, 23.06, 23.04, 22.80, 22.78, 20.43, 20.37, 20.30, 20.24, 20.17, 20.12, 14.17, 14.15. ³¹P NMR (202 MHz, CDCl₃): δ = 149.34, 148.94. HRMS (ESI, positive) *m/z*: [M+Na]⁺ calc. for [C₅₅H₆₁N₄O₈SPNa]⁺: 991.3840, found: 991.3814.

Table S7: Nucleotide modification.

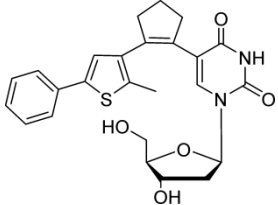
modified nucleoside	acronym	description
	dU^{PS}	Deoxyuridine-based photoswitchable nucleoside with phenyl substituent

Table S8: Mass, sequence and chemical formula of the synthesized oligonucleotides.

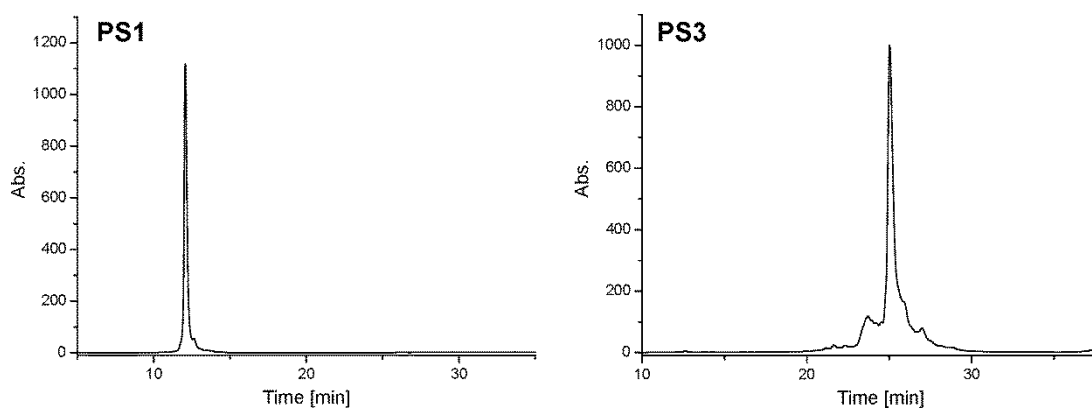
Name	Sequence	chemical formula	calculated mass [m/z]	found mass [m/z]
PS1	GGC TAG CTA CdU ^{PS} A CGA	C ₁₆₁ H ₁₉₆ N ₅₈ O ₈₇ P ₁₄ S ₁	4800.8807	4800.8795
PS3	GGC TAG CdU ^{PS} A CdU ^{PS} A CdU ^{PS} A	C ₁₉₁ H ₂₂₁ N ₅₅ O ₈₈ P ₁₄ S ₃	5224.0049	5223.9483

Table S9: Gradients for preparative HPLC purification of the synthesized oligonucleotides

Method A		Method B	
Time [min]	Buffer B [%]	Time [min]	Buffer B [%]
0	10	0	5
5	20	2	5
10	30	7	15
35	40	22	20
40	100	29	40
42	10	35	60
		45	100
		55	5

Table S10: HPLC gradient for LC/MS measurements

Method C	
Time [min]	Methanol [%]
0	10
5	20
10	30
35	40
40	100
42	10

**Figure S7:** HPLC chromatograms of the synthesized oligonucleotides with one modification (**PS1**) and three modifications (**PS3**), detected at 280 nm.

REFERENCES

1. Lakowicz, J. R., *Principles of Fluorescence Spectroscopy*, (1999). Kluwer Academic/Plenum Publishers, New York: 2004; pp 55-56.
2. Reichardt, C., Solvatochromic Dyes as Solvent Polarity Indicators. *Chem. Rev.* **1994**, *94*, 2319-2358.
3. Irie, M.; Fukaminato, T.; Matsuda, K.; Kobatake, S., Photochromism of Diarylethene Molecules and Crystals: Memories, Switches, and Actuators. *Chem. Rev.* **2014**, *114*, 12174-12277.
4. Lee, J.-H., Bulk FinFETs: Design at 14-nm Node and Key Characteristics. In *Nano Devices and Circuit Techniques for Low-Energy Applications and Energy Harvesting*, Springer: New York, 2016; pp 33-64.
5. Sugii, N., Low-Power Electron Devices. In *Green Computing with Emerging Memory*, Springer: 2013; pp 9-33.
6. Parikh, P.; Senowitz, C.; Lyons, D.; Martin, I.; Prosa, T. J.; DiBattista, M.; Devaraj, A.; Meng, Y. S., Three-Dimensional Nanoscale Mapping of State-of-the-Art Field-Effect Transistors (FinFETs). *Microsc. Microanal.* **2017**, *23*, 916-925.
7. Masuhara, T., The Future of Low-Power Electronics. In *Chips 2020*, Springer: New York, 2016; Vol. 2, pp 21-50.
8. Lubow, A.; Ismail-Beigi, S.; Ma, T. P., Comparison of Drive Currents in Metal-Oxide-Semiconductor Field-Effect Transistors Made of Si, Ge, GaAs, InGaAs, and InAs Channels. *Appl. Phys. Lett.* **2010**, *96*, 122105.
9. Sicard, E., Introducing 14-nm FinFET Technology in Microwind. Hyper Articles en Ligne (HAL), hal-01541171, **2017**, 25.
10. Shim, S.; Joo, T.; Bae, S. C.; Kim, K. S.; Kim, E., Ring Opening Dynamics of a Photochromic Diarylethene Derivative in Solution. *J. Phys. Chem. A* **2003**, *107*, 8106-8110.
11. Shim, S.; Eom, I.; Joo, T.; Kim, E.; Kim, K. S., Ring Closure Reaction Dynamics of Diarylethene Derivatives in Solution. *J. Phys. Chem. A* **2007**, *111*, 8910-8917.
12. Ansari, M.; Afzali-Kusha, H.; Ebrahimi, B.; Navabi, Z.; Afzali-Kusha, A.; Pedram, M., A near-Threshold 7T SRAM Cell with High Write and Read Margins and Low Write Time for Sub-20 nm FinFET Technologies. *INTEGRATION, the VLSI journal* **2015**, *50*, 91-106.